Simulation of Blood Flow in Patient-specific Cerebral Arteries with a Domain Decomposition Method

Wen-Shin Shiu, Zhengzheng Yan, Jia Liu, Rongliang Chen, Feng-Nan Hwang, and Xiao-Chuan Cai

1 Introduction

The high morbidity and mortality of stroke has caused a social and economic burden in contemporary society. The underlying mechanisms of stroke are not fully understood. Changes of cerebral hemodynamics might be one of the critical factors that cause stroke. There are several techniques to detect the hemodynamic alterations, one of which is through computer simulation by solving partial differential equations that describe the physics of the blood flow. For example, there are some numerical studies of blood flow through a total cavopulmonary connection (Bazilevs et al., 2009), the coronary (Taylor et al., 2013), cerebral aneurysms (Boussel et al., 2009; Cebral et al., 2005; Takizawa et al., 2011), and cerebrovascular arteries, which is the focus of this paper (Moore et al., 2005). In general, solving a fluid flow problem with complex geometry in 3D is difficult. In this work, we employ a Newton-Krylov-Schwarz (NKS) algorithm for solving large nonlinear systems arising from a fully implicit discretization of the incompressible Navier-Stokes equations using the Galerkin/least squares (GLS) finite element method. NKS has

W.-S. Shiu (✉) • Z. Yan • J. Liu • R. Chen
Shenzhen Institutes of Advanced Technology, Chinese Academy of Sciences, Shenzhen 518055, Guangdong, People's Republic of China
e-mail: whsin5@gmail.com; zz.yan@siat.ac.cn; jia.liu@siat.ac.cn; rl.chen@siat.ac.cn

F.-N. Hwang
Department of Mathematics, National Central University, Jhongli District, Taoyuan City 32001, Taiwan
e-mail: hwangf@math.ncu.edu.tw

X.-C. Cai
Department of Computer Science, University of Colorado, Boulder, CO 80309, USA
e-mail: cai@cs.colorado.edu

been applied for simple blood flow model problems previously (Hwang et al., 2010). In this work, we apply the algorithm to a patient-specific cerebrovascular problem that is more complicated, since the cerebrovascular artery has ischaemic stenosis, and the vessel wall is atherosclerotic. The rest of the paper is organized as follows. In the next section, we provide a description of the governing equations of blood flow in cerebral arteries, the finite element discretization, and the parallel NKS based solution algorithm. In Sect. 3, numerical results and parallel performance study are presented. Some concluding remarks are given in Sect. 4.

2   Blood Flow Model, Discretization, and Solution Algorithm

We assume that the blood flow is isothermal, incompressible, Newtonian and laminar, and modeled by the unsteady Navier-Stokes equations,

$$
\begin{cases}
\rho \left(\dfrac{\partial \boldsymbol{u}}{\partial t} + \boldsymbol{u} \cdot \nabla \boldsymbol{u} \right) - \nabla \cdot \boldsymbol{\sigma} = 0 & \text{in } \Omega \times (0, T), \\
\nabla \cdot \boldsymbol{u} = 0 & \text{in } \Omega \times (0, T), \\
\boldsymbol{u} = 0 & \text{on } \Gamma_{wall} \times (0, T), \\
\boldsymbol{u} = g & \text{on } \Gamma_{in} \times (0, T), \\
\sigma \cdot \boldsymbol{n} = \boldsymbol{0} & \text{on } \Gamma_{out} \times (0, T), \\
\boldsymbol{u} = \boldsymbol{u}_0 & \text{in } \Omega \text{ at } t = 0,
\end{cases}
\tag{1}
$$

where $\boldsymbol{u}=(u_1, u_2, u_3)^T$ is the velocity field, ρ is the fluid density, and $\boldsymbol{\sigma}$ is the Cauchy stress tensor defined as $\boldsymbol{\sigma} = -p\boldsymbol{I} + 2\mu\boldsymbol{D}$, where p is the pressure, $\boldsymbol{I}$ is the identity tensor, μ is dynamic viscosity, and the deformation rate tensor $\boldsymbol{D} = \frac{1}{2}[\nabla \boldsymbol{u} + (\nabla \boldsymbol{u})^T]$. $\Omega \in R^3$ is the computational domain, with three boundaries Γ_{in}, Γ_{out} and Γ_{wall}; Γ_{in} is the surface of the inlet, Γ_{out} contains the surfaces of all outlets, and Γ_{wall} is the vessel wall. To close the flow system, some proper boundary conditions need to be imposed. We impose a uniform velocity, g, for the velocity on Γ_{in}; a stress-free boundary condition on Γ_{out}, and a no-slip boundary condition on Γ_{wall}.

To discretize (1), we employ a $P_1 - P_1$ GLS finite element method for the spatial domain, and an implicit first-order backward Euler scheme for the temporal domain (Wu and Cai, 2014). The GLS finite element takes the following form (Franca and Frey, 1992): Find $\boldsymbol{u}_h^{(n+1)} \in V_h^g$ and $p_h^{(n+1)} \in P_h$, such that

$$
B(\boldsymbol{u}_h^{(n+1)}, p_h^{(n+1)}; \boldsymbol{v}, q) = 0, \quad \forall (\boldsymbol{v}, q) \in V_h^0 \times P_h
$$

with

$$B(\boldsymbol{u}, p; \boldsymbol{v}, q) = \left(\frac{\boldsymbol{u} - \boldsymbol{u}^{(n)}}{\Delta t} + (\nabla \boldsymbol{u})\boldsymbol{u}, \boldsymbol{v} \right) + (\nu \nabla \boldsymbol{u}, \nabla \boldsymbol{v}) - (\nabla \cdot \boldsymbol{v}, p)$$
$$+ \sum_{K \in \mathcal{T}^h} \left(\frac{\boldsymbol{u} - \boldsymbol{u}^{(n)}}{\Delta t} + (\nabla \boldsymbol{u})\boldsymbol{u} + \nabla p, \tau_{GLS}((\nabla \boldsymbol{v})\boldsymbol{u} - \nabla q) \right)_K$$
$$- (\nabla \cdot \boldsymbol{u}, q) + (\nabla \cdot \boldsymbol{u}, \delta_{GLS} \nabla \cdot \boldsymbol{v}),$$

where V_h^0 and V_h^g are the weighting and trial velocity function spaces respectively. P_h is a linear finite element space for the pressure and used for both the weighting and trial pressure function spaces. $\boldsymbol{u}^{(n)}$ is the velocity vector at the current time step, and $\boldsymbol{u}$ and p (we drop the superscript $(n+1)$ here for simplicity) are unknown velocity and pressure at the next time step. ν is the kinematic viscosity. Δt is the time step size. Note that $\mathcal{T}^h = \{K\}$ is a tetrahedral mesh. We use the stabilization parameters τ_{GLS} and δ_{GLS} suggested in Franca and Frey (1992). The GLS formulation can be written as a nonlinear algebraic system

$$F(x) = 0, \tag{2}$$

where x is the vector of nodal values of the velocity and the pressure.

We apply NKS to solve (2). NKS is an inexact Newton method in which the Jacobian systems are solved by an one-level Schwarz preconditioned Krylov subspace method, briefly described as follows: Let $x^{(k)}$ be the current approximation of x, and $x^{(k+1)}$ the new approximation computed by the substeps:

Step 1: Solve the following preconditioned Jacobian system approximately by GMRES to find a Newton direction $s^{(k)}$,

$$J_k M_k^{-1} y = -F(x^{(k)}), \text{ with } s^{(k)} = M_k^{-1} y, \tag{3}$$

where J_k is the Jacobian of F evaluated at Newton step k, and M_k^{-1} is a right preconditioner.
Step 2: Obtain the new approximation with a linesearch method,

$$x^{(k+1)} = x^{(k)} + \lambda^{(k)} s^{(k)}, \tag{4}$$

where $\lambda^{(k)}$ is a step length parameter.

We define the additive Schwarz preconditioner in the matrix form as

$$M_k^{-1} = \sum_{i=1}^{N} (R_i^h)^T J_i^{-1} R_i^h,$$

where J_i^{-1} is the inverse of the subspace Jacobian $J_i = R_i^h J (R_i^h)^T$. We denote R_i^h as the global-to-local restriction operator and $(R_i^h)^T$ as the local-to-global prolongation operator. The multiplication of J_i^{-1} with a vector is solved by a direct solver such as sparse LU decomposition or an inexact solver such as ILU with some level of fill-ins.

3   A Case Study and Discussions

We consider a pair of patient-specific cerebrovascular geometries provided by the Beijing Tiantan Hospital, as shown in Fig. 1. The pair of cerebral arteries belongs to the same patient before and after the cerebral revascularization surgery respectively. In Fig. 1, the left artery has a stenosis in the middle, the right figure shows the same artery after the stenosis is surgically removed. Our numerical simulations provide a valuable tool to understand the change of the dynamics of the blood flow in the patient and the impact of the surgery. For convenience, let us denote the artery with a stenosis as "pre" and the repaired artery as "post". Table 1 lists the number of vertices, elements and unknowns of the finite element meshes that we generate for solving the flow problems.

The blood flow is characterized with density $\rho = 1.06\,\text{g/cm}^3$, and viscosity $\mu = 0.035\,\text{g/(cm} \cdot \text{s)}$. The inflow velocity profile is shown in Fig. 2. The time step size is $\Delta t = 10^{-2}\,\text{s}$. For the algorithm parameters, the overlapping size for the Schwarz preconditioner is set to be $\delta = 1$, and subdomain linear system is solved by ILU(1). The Jacobian system is solved inexactly by using an additive Schwarz preconditioned GMRES with relative stopping condition 10^{-4}. We define Newton convergence with a relative tolerance of 10^{-6} or an absolute tolerance of 10^{-10}. To observe the behavior of the blood flow in systolic and diastolic phases,
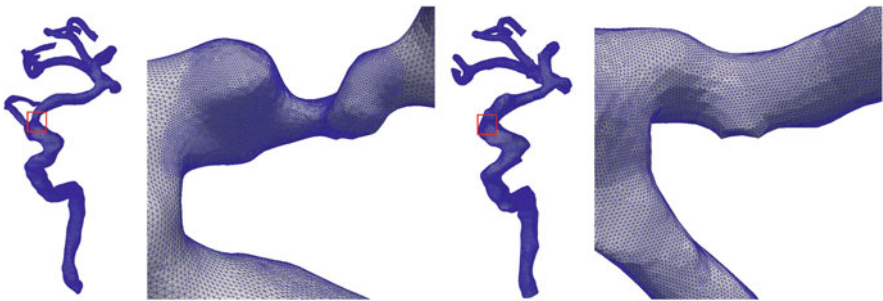

Fig. 1 3D tetrahedral meshes before and after the surgery. The narrowing cerebral artery with a local refinement at the stenosed segment (*left*) and the repaired cerebral artery (*right*)

Table 1 Mesh information for two cerebrovascular geometries

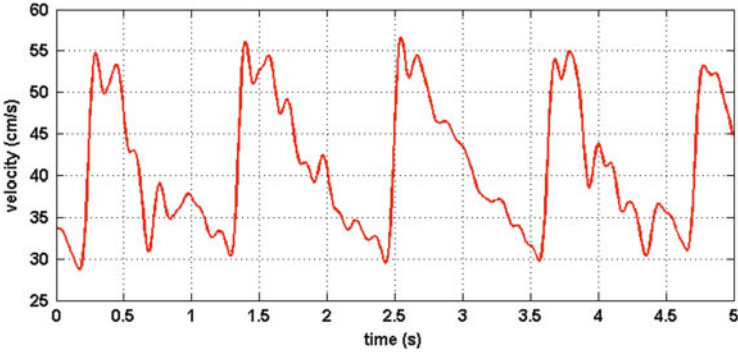| Mesh	# of vertices	# of elements	# of unknowns
Pre	441,475	2,208,337	1,765,900
Post	287,936	1,360,588	1,151,744

Fig. 2 Inflow velocity profile for 5 cardiac cycles discretized with 500 time steps

we respectively plot the numerical solutions at $t = 2.54$ s and $t = 3.2$ s. Figure 3 shows the relative pressure distributions, and Fig. 4 shows the streamlines whose color indicates the velocity magnitude.

We focus on the comparison between the "pre" and "post" cases. Figure 3 shows that the range of the relative pressure value of the "pre" case is more than double that of the "post" case at the systolic and diastolic phases. Moreover, as shown in the same figure, the relative pressure ratio between the anterior and posterior parts of the stenosed portion in the "pre" case is large, and the relative pressure value of the "post" case at the repaired portion has a smaller variation. From the streamline plots, the blood flow is more disordered in the "pre" case than in the "post" case during both the diastolic period and the systolic period. In addition, the maximum of the velocity occurs at the stenosed portion in the "pre" case, and the variation of the velocity distributions in the repaired portion is quite small. Similar to the pressure distribution, the range of velocity magnitude of the "pre" case is wider than the "post" case.

We use the "post" case to test the parallel performance, and the simulation is carried out for 10 time steps. Numerical results are summarized in Table 2. "np" is the number of processor cores. "NI" denotes the number of Newton iterations per time step, "LI" denotes the average number of GMRES iterations per Newton step, "T" represents the total compute time in seconds and "EFF" is the parallel efficiency. It is clear that for the iteration counts, the algorithm is not sensitive to the overlapping size δ. For fixed np, the number of average GMRES iterations decreases as the levels of fill-ins increases. The number of Newton iterations is
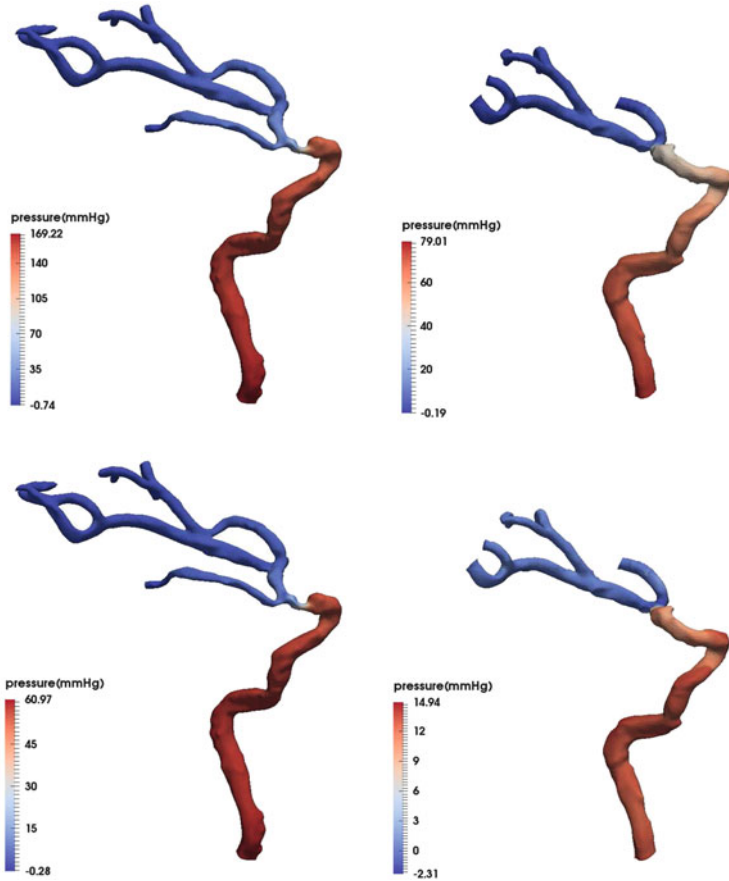
Fig. 3 Relative pressure distributions at $t = 2.54$ s (*top*) and $t = 3.2$ s (*bottom*) for pre (*left*) and post (*right*)

almost independent of the overlapping size for the Schwarz preconditioner and levels of fill-ins of subdomain solvers, and the average number of GMRES iterations increases slightly as the number of processor cores grows. Hence, we claim that NKS is quite robust for the test cases presented in this paper. For the best algorithmic parameter selection of ILU fill level 2, and small overlap of 0 or 1, about 70% relative efficiency is achieved in strong scaling between 32 and 128 processor cores.
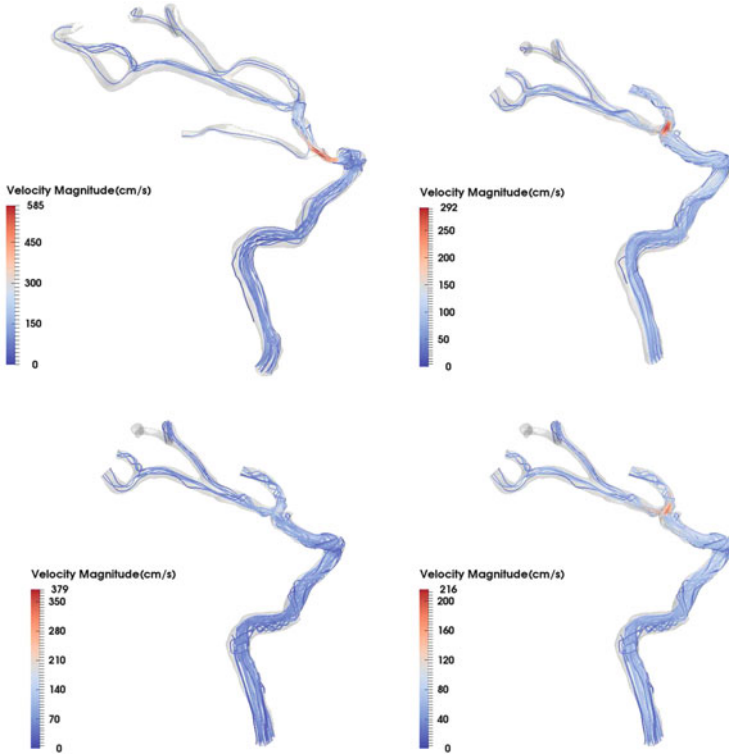
Fig. 4 Streamlines at $t = 2.54$ s (*top*) and $t = 3.2$ s (*bottom*) for pre (*left*) and post (*right*)

4   Concluding Remarks

We simulated blood flows in a pair of patient-specific cerebral arteries during 5 cardiac cycles by a fully implicit finite element discretization method and a Newton-Krylov-Schwarz algebraic solver. The simulations show clearly that the physics of the blood flow is more complicated before the surgery than after the surgery, and the stenosis causes a large variation of the pressure and velocity field. As to the NKS algorithm itself, we showed that the algorithm is robust with respect to the overlapping size for the Schwarz preconditioner and levels of fill-ins of subdomain solvers. A reasonably good scalability is observed with up to 128 processor cores.

Table 2 Parallel performance of NKS with up to 128 processor cores

np	Subsolver	δ	NI	LI	T	EFF (%)
32	ILU(0)	0	3	820.5	2860	100
		1	3	814.1	2650	100
		2	3	832.3	2805	100
		3	3	838.2	2761	100
	ILU(1)	0	2.9	351.8	1698	100
		1	2.9	351.9	1717	100
		2	2.9	360.7	1741	100
		3	2.9	366.5	1805	100
	ILU(2)	0	2.8	248.2	1563	100
		1	2.8	248.1	1666	100
		2	2.8	247.1	1600	100
		3	2.8	251.2	1663	100
64	ILU(0)	0	2.9	828.1	1438	99
		1	2.9	828.1	1413	94
		2	3	839.3	1495	94
		3	3	845.1	1527	90
	ILU(1)	0	2.9	384.2	966	88
		1	2.9	384.4	973	88
		2	2.9	372.0	970	90
		3	2.9	388.2	1042	87
	ILU(2)	0	2.8	289.5	931	84
		1	2.8	290.1	920	91
		2	2.8	266.3	906	88
		3	2.8	266.3	941	88
128	ILU(0)	0	3	842.9	845	85
		1	3	843.0	836	79
		2	3.6	876.5	1089	64
		3	3.9	914.0	1584	44
	ILU(1)	0	2.9	428.7	610	70
		1	2.9	428.2	617	70
		2	2.9	437.1	719	60
		3	2.9	443.1	932	48
	ILU(2)	0	2.8	324.8	570	69
		1	2.8	324.8	572	73
		2	2.8	300.9	583	69
		3	2.8	286.2	596	70

References

Y. Bazilevs, M.-C. Hsu, D.J. Benson, S. Sankaran, A.L. Marsden, Computational fluid–structure interaction: methods and application to a total cavopulmonary connection. Comput. Mech. **45**, 77–89 (2009)

L. Boussel, V. Rayz, A. Martin, G. Acevedo-Bolton, M.T. Lawton, R. Higashida, W.S. Smith, W.L. Young, D.S. Saloner, Phase-contrast MRI measurements in intracranial aneurysms in vivo of flow patterns, velocity fields, and wall shear stress: comparison with CFD. Magn. Reson. Med. **61**, 409–417 (2009)

J.R. Cebral, M.A. Castro, S. Appanaboyina, C.M. Putman, D. Millan, A.F. Frangi, Efficient pipeline for image–based patient–specific analysis of cerebral aneurysm hemodynamics: technique and sensitivity. IEEE Trans. Med. Imaging **24**, 457–467 (2005)

L.P. Franca, S.L. Frey, Stabilized finite element methods. II: the incompressible Navier–Stokes equations. Comput. Methods Appl. Mech. Eng. **99**, 209–233 (1992)

F.-N. Hwang, C.-Y. Wu, X.-C. Cai, Numerical simulation of three–dimensional blood flows using domain decomposition method on parallel computer. J. Chin. Soc. Mech. Eng. **31**, 199–208 (2010)

S.M. Moore, K.T. Moorhead, J.G. Chase, T. David, J. Fink, One–dimensional and three–dimensional model of cerebrovascular flow. Biochem. Eng. J. **127**, 440–449 (2005)

K. Takizawa, C. Moorman, S. Wright, J. Purdue, T. McPhail, P.P. Chen, J. Warren, T.E. Tezduyar, Patient–specific arterial fluid–structure interaction modeling of cerebral aneurysms. Int. J. Numer. Meth. Fluids **65**, 308–323 (2011)

C.A. Taylor, T.A. Fonte, J.K. Min, Computational fluid dynamics applied to cardiac computed tomography for noninvasive quantification of fracional flow reserve. J. Am. Coll. Cardiol. **61**, 2233–2241 (2013)

Y. Wu, X.-C. Cai, A fully implicit domain decomposition based ALE framework for three-dimensional fluid–structure interaction with application in blood flow computation. J. Comput. Phys. **258**, 524–537 (2014)